Mem. Natl Inst. Polar Res., Spec. Issue, **54**, 9–20, 2001

Scientific paper

Observations of the polar *D*-region and the mesosphere with the EISCAT Svalbard Radar and the SOUSY Svalbard Radar

Jürgen Röttger

Max-Planck-Institut für Aeronomie, D-37191 Katlenburg-Lindau, Germany
(roettger@linmpi.mpg.de)

Abstract: Two new radars are operated at high polar latitudes on Svalbard, the EISCAT Svalbard Radar (ESR) and the SOUSY Svalbard Radar (SSR). The application of these systems for studies of Polar Mesosphere Summer Echoes (PMSE) is described. The ESR is also used for studies of the *D*-region using the incoherent scatter method. Combined observations with these two radars yield insight into the wavenumber dependence of the scatter cross section, which in turn leads to indications on the diffusion of electrons in the presence of heavy ions.

1. Introduction

The polar middle atmosphere is of unique nature, since in that region processes from above (solar wind–magnetosphere–ionosphere–thermosphere) and from below (troposphere–stratosphere–mesosphere–lower thermosphere) merge. Röttger (1994a) and Röttger and Tsuda (1995) have summarized the contributions of incoherent scatter and MST radars to study these processes. In particular the effects of Joule heating and high energetic particles on the lower thermosphere and upper mesosphere wind and temperature fields, the interaction of the neutral and ionized middle atmosphere during particle precipitation and the presence of aerosols, cluster ions and ice particles in the cold polar mesopause in summer are of special interest. The effect of planetary waves, tides, gravity waves and turbulence on the polar middle atmosphere at not very well known either. The archipelago of Svalbard at high polar latitudes close to 80°N is a unique location to study many of these processes.

Of great importance are the Polar Mesosphere Summer Echoes (see Cho and Röttger, 1997, for a review), which had not been studied at the high latitudes of Svalbard. Besides their relation to electron density, the Polar Mesosphere Summer Echoes (PMSE) are strongly dependent on temperature and water vapor mixing ratio. These parameters vary with latitude. Hemispheric differences of PMSE are also reported (Balsley *et al.*, 1995), which may indicate temperature differences between the Arctic and the Antarctic mesopause. Comparisons of PMSE observations on Svalbard with those at lower latitudes and in the southern hemisphere will consequently be very valuable. The PMSE distinctly depend on the wavenumber of the probing radar. Combined observations with radars on different frequencies, such as the EISCAT Svalbard Radar (Wannberg *et al.*, 1997; Röttger *et al.*, 1998) and the SOUSY Svalbard Radar (Czechowsky *et al.*, 1998; Röttger, 2000), are mandatory to understand the scattering mechanism and the governing spatial irregularity

structure causing PMSE. The fairly continuous appearance of the PMSE can properly be used to study dynamic processes, such as long period waves, tides, gravity waves and turbulence, which occur in the high latitude mesopause region.

In this paper early observations of the *D*-region and mesopause region with the ESR and the SSR are described. Observations of the lower stratosphere and the troposphere are presented in the companion paper (Röttger, 2001).

2. The EISCAT Svalbard Radar

During our initial *D*-region experiments in 1998 and 1999 the EISCAT Svalbard Radar (ESR), which is an incoherent scatter radar operated on 500 MHz, a peak power between 500 kW or 1000 kW was transmitted using the 32 m parabolic dish antenna. It is estimated that in this particular experiment configuration the smallest detectable electron density is close to 3×10^8 m^{-3} for maximum integration times in the order of minutes. This would be decreased by about a factor of two with the second antenna, which is now available at the EISCAT Svalbard Radar (Fig. 1).

Due to longer coherence time of echoes from the lower ionosphere the pulse-to-pulse modulation has to be applied (Röttger, 1997). It is suitable to implement the complementary code to increase the average transmitted power and thus the significance of the result estimates. Röttger *et al.* (1998) have described the operational mode of the ESR for these observations. The technical details of the whole ESR system have been published by Wannberg *et al.* (1997).

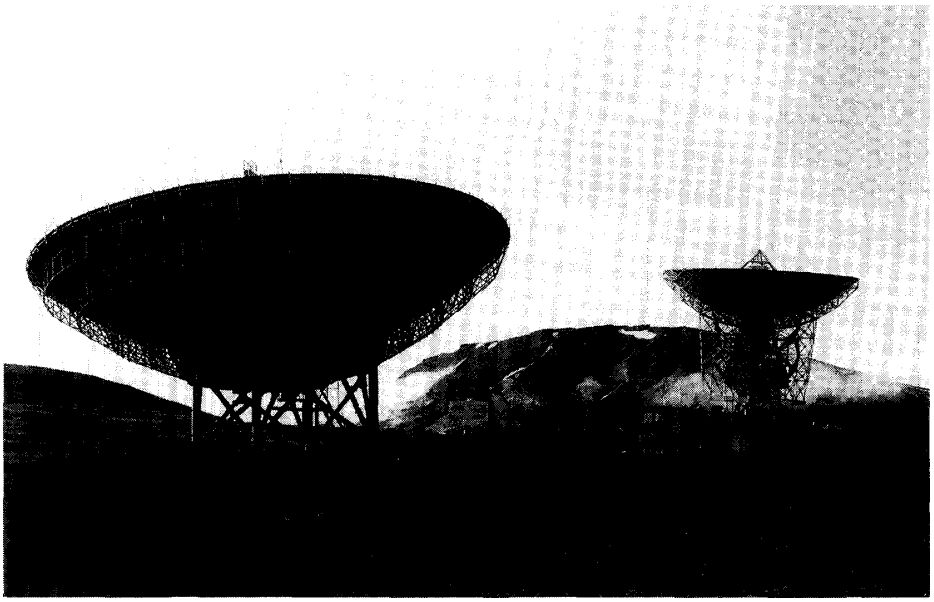

Fig. 1. The EISCAT Svalbard Radar (ESR) with the 32-m steerable dish in the background and the 42-m fixed dish in the foreground (September 1999).

3. The SOUSY Svalbard Radar

The SOUSY Svalbard Radar (SSR) is an MST radar and was particularly conceived for the studies of Polar Mesosphere Summer Echoes (Czechowsky *et al.*, 1998). This radar uses the main basic components of the mobile SOUSY VHF radar, combined with a new phased-antenna array of 356 Yagis (Fig. 2). The antenna can be steered to five beam directions: the zenith, and to 5 degrees zenith angle in NE, SE, SW, and NW azimuths. The SSR operates at 53.5 MHz and was run at a peak power around 70 kW during several campaigns in 1999, applying the complementary code. Röttger (2000) has preliminarily summarized the basic results of these first operations, which consisted of PMSE, meteor and stratosphere-troposphere programs, and Rüster *et al.* (2001) have described some typical features of PMSE, such as their double layer structure and the wind field in the mesopause region.

The SOUSY Svalbard Radar (SSR) is located in very close vicinity of the EISCAT Svalbard Radar (ESR), which allows well coordinated experiment operations for observations of the mesosphere, and the *D*- and *E*-region, which are of great importance to understand the aeronomy and dynamics of the upper middle atmosphere (say, 50 km to 100 km altitude) at high polar latitudes.

A summary of the system parameters of the SSR and ESR, relevant for these particular studies, is given in Table 1. Both these radars are located at 78°N, 16°E.

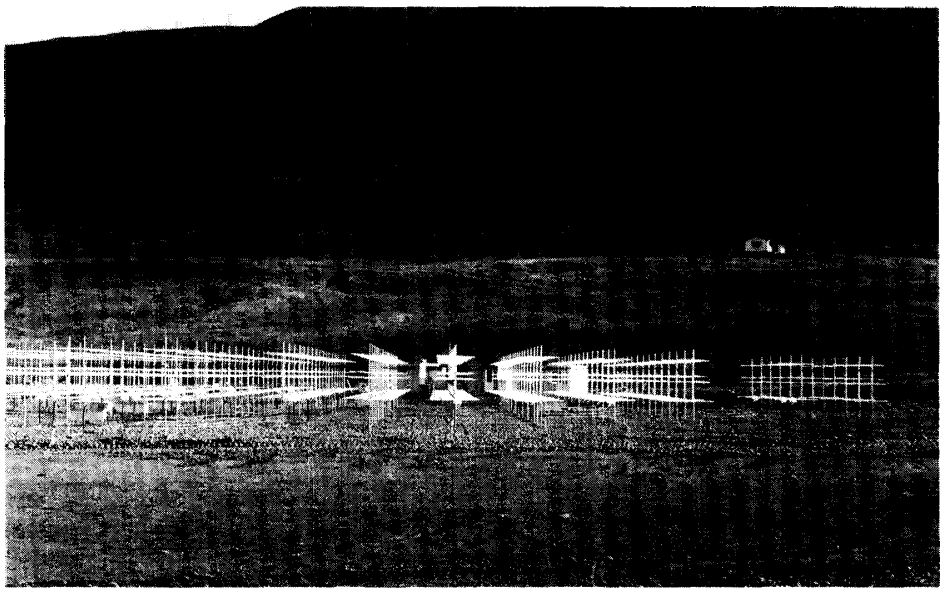

Fig. 2. The SOUSY Svalbard Radar (SSR) with the phased array consisting of a total of 356 Yagi antennas (September 1998).

Table 1. System parameters of the EISCAT Svalbard Radar (ESR) and the SOUSY Svalbard Radar (SSR).

System parameters	ESR	SSR
Antenna gain G in dBi	42.5	33.0
Half power beam width Θ	1.23°	4.0°
Frequency f in MHz	500	53.5
Wavelength λ in m	0.60	5.61
Peak power P_p in MW	0.8	0.07
Duty cycle d	0.14	0.04
Average power P_a in kW	115	2.8
Number n_b of code bauds	32	20
Effective power $2 \cdot P_p \cdot n_b$ in MW	51.2	2.4
System efficiency (assumed)	0.8	0.8
Pulse (baud) length τ in μs	6	2
System temperature T_s in K	70	3000
Number coherent integrations n_{coh}	2	4×21
Detection bandwidth f_b in kHz	83.3	2.98
System figure of merit F_m	$1 \cdot 10^{23}$	$6 \cdot 10^{22}$
Minimum detectable radar reflectivity η in m^{-1}	$2.6 \cdot 10^{-19}$	$7.5 \cdot 10^{-19}$

4. Observations of incoherent scatter from the lower ionosphere with the ESR

Incoherent scatter from the lower ionosphere (mesosphere) is collision dominated. This means that the spectra are approaching Lorentzian shape, rather than displaying the double-hump shape of the spectra from the *E*- and *F*-region. The spectrum width in the collision-dominated regime is a measure of temperature and density of the neutral atmosphere, and the Doppler shift is a direct measure of the neutral air velocity. The scattered power is in the first order proportional to the electron density. Since this is usually fairly low in the *D*- and lower *E*-region, the scattered signal is very weak. This means that either long integration times have to be applied to obtain significant estimates of the given parameters or ionization increases need to occur during ionospheric disturbances. In the polar cap (Svalbard is located in the polar cap) usually energetic particle precipitation during solar proton events enhance the *D*-region density, which allow integration times of less than one minute.

The first tests of *D*-region observations with the ESR (Röttger *et al.*, 1998) were during the declining phase of a solar proton event and signals could be detected at significant levels. Figure 3 shows examples of dynamic spectra (left-hand panels) of echoes from the lower *D*-region at altitudes between 54 km and 64 km, which were detected on 24 April 1998. The right-hand side displays the corresponding scatter plots of the spectra. The peak signal power is in the order of the variance of the background noise and the signal-to-noise ratio is a few percent only. To obtain reasonable estimates of electron density and velocity, thus, requires a few minutes of post-integration of the spectra. This allows to studying short-term variations of the *D*-region, for instance during solar proton events. Indications of such variations are seen in the development of the dynamic spectra as function of height and time. We note some quasi-periodic variation of the spectral power, *i.e.* electron density,

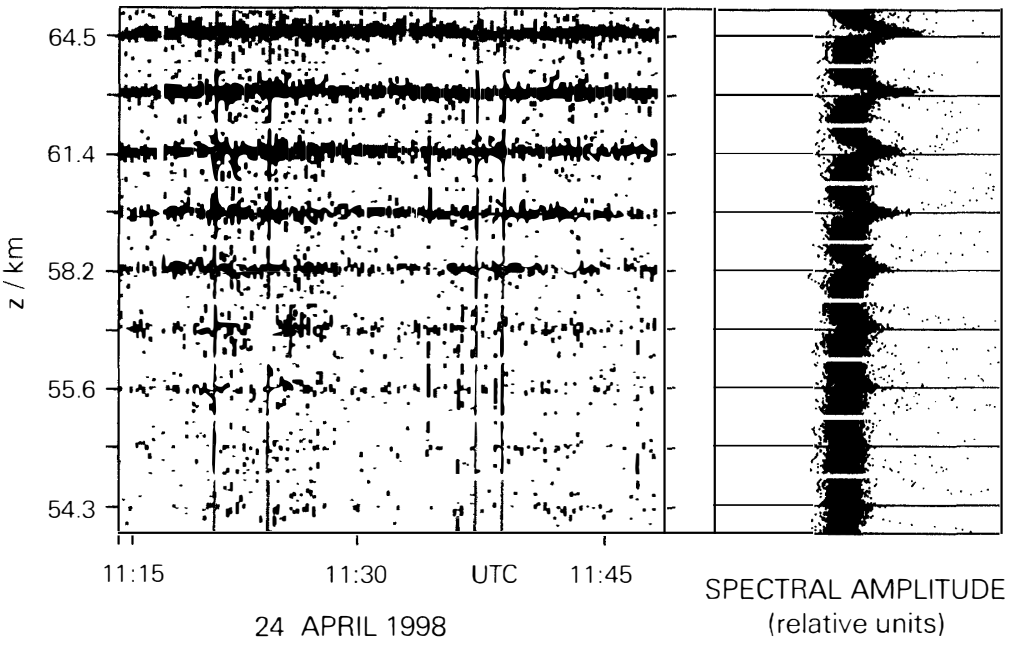

Fig. 3. Dynamic spectra (left-hand panels) of incoherent scatter signals from the lower D-region detected by the ESR on 24 April 1998 during the decaying phase of a solar proton event. On the right hand-panels the scatter plots of the spectra for the total time period are shown. The Doppler velocity limits of the spectra are $\pm 111\ m\,s^{-1}$.

below about 60 km in Fig. 3 with maxima around 1125 UT and 1140 UT.

At higher altitudes the signal-to-noise ratio improves, which can be seen in another example (Fig. 4), where data taken with the ESR on 15 July 1999 are presented. This operation was during a campaign to search for PMSE. The upper panel shows the height-time-intensity plot and the scatter profile of the raw power estimate between 78 and 101 km altitude, which was recorded between 1315 and 1325 UT. The raw power estimate represents a first-order estimate of the yet uncalibrated electron density profile. A gradual weak increase of the raw power is noticed to occur above about 85 km. The raw power then increases significantly above 90 km, which comprises the lower *E*-region. There is even an indication of a sporadic-*E* or ion layer around 95 km. Due to the applied pulse-to-pulse modulation using the complementary code (optimized for PMSE detection), the incoherent scatter signals from heights above about 88 km are aliased. Thus, full spectra cannot be obtained, but the power is a proper first-order estimate of the electron density, since coherent integration was not applied in our experiments.

Particular narrow lines occur in the spectra at altitudes 88–89 km in Fig. 4. These are features of Polar Mesosphere Summer Echoes, which will be discussed further in the following chapter. Röttger (2000) has described more details of these first PMSE observations with the ESR, and Hall and Röttger (2001) discussed their occurrence frequency and further principle features. In the following we present and discuss scatter cross section comparisons of common PMSE observations with the ESR and the SSR, which will provide an indication on the presence of aerosols and ice particles.

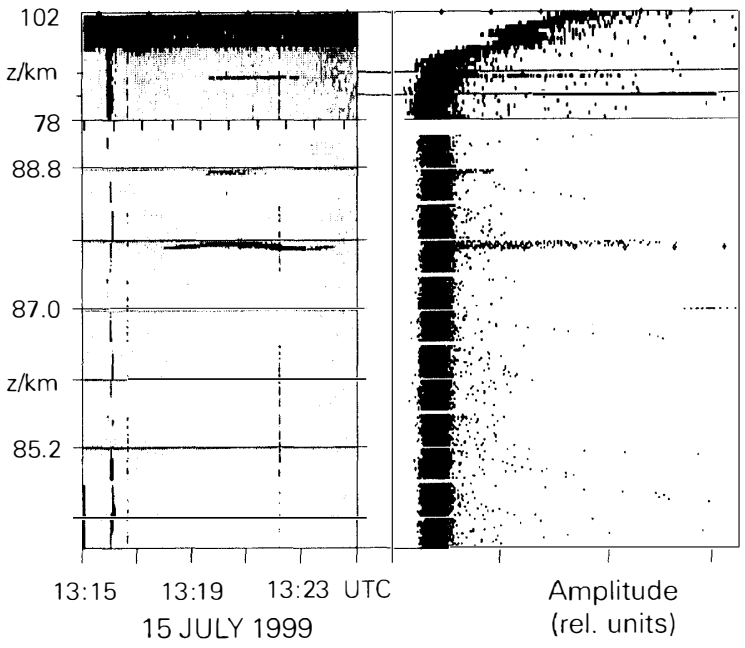

Fig. 4. Left-hand panels: Height-time intensity plot of signals from the D-region and lower E-region (upper plot), and six dynamic spectra of signals from the height ranges embraced by the tick marks/lines the upper diagrams. The straight lines in the dynamic spectra indicate zero velocity. The velocity limits are $\pm 111\ m\,s^{-1}$.
Right-hand panels: Scatter plots of the parameters in the left-hand panels.

5. Observations of Polar Mesosphere Summer Echoes with the ESR and SSR

Whereas incoherent scatter results from electrons in thermal equilibrium (thermal scatter), in particular conditions, such as large cluster ions and other particles in the mesopause region, the incoherent scatter process is changed substantially. This process can be called non-thermal scatter. The scattered signal exhibits a highly coherent nature and its amplitude exceeds the common incoherent and turbulence scatter level by many orders of magnitude. This is seen in the narrow spectral lines, occurring in narrow height slices, as displayed in Fig. 4. These echoes, called Polar Mesosphere Summer Echoes (PMSE), occur in the very cold high-latitude mesopause and are related to the formation of ion clusters and ice particles. They should not be confused with the common coherent scatter echoes, which are detected by MST radars, and which result from neutral-turbulence induced irregularities in the *D*-region/mesosphere. Although the difference between the scatter causing the PMSE and the conventional incoherent and turbulence scatter from the mesosphere is generally agreed upon, the scattering process occurring during the PMSE conditions is not fully explained yet (*e.g.,* Cho and Röttger, 1997; Klostermeyer, 1999).

PMSE had been observed over a wide range of frequencies (Röttger, 1994b), corresponding to radar wavelengths of 100 m to 0.25 m. Some comparisons of the phenomenology of PMSE had been done using data obtained with collocated radars (*e.g.,*

Röttger *et al*., 1990; Bremer *et al*., 1996), but finally robust estimates of scatter cross sections during concurrent observations and comparisons with model results were not yet done. This was first performed using data acquired in 1999 with the SOUSY Svalbard Radar and the EISCAT Svalbard Radar, and is briefly described here.

In July 1999 these two radars were partly operated simultaneously to search for events when PMSE occurred on the frequencies 53.5 MHz (SSR) and 500 MHz (ESR). Such a comparison should allow indications about the scattering process, *i.e.* whether the 500 MHz scatter would be enhanced Thomson scatter by dressed particles, enhancement of the particle line of modified Thomson scatter or enhancement due to an increase of the Schmidt number (for references see Röttger, 1994b; Cho and Röttger, 1997; Klostermeyer, 1999). A conclusion in turn would allow indications on the microphysics of the scattering medium, for instance whether there are multiply charged aerosols, reduced electron diffusion in the presence of heavy ions, or just enhanced neutral turbulence. The latter, however, is believed to be excluded since neutral turbulence in the mesopause region does not extend to short scales matching the Bragg wavelengths of these two radars.

The decrease of the scatter cross section of PMSE as function of the spatial wave number, given by the conventionally applied spectrum, dictates that there should be a several orders of magnitude smaller cross section on 500 MHz than on 53.5 MHz (Kelley *et al*., 1987). To estimate whether such a search for PMSE on 500 MHz would be successful we first need to compare the corresponding system parameters of the SSR and the ESR. This comparison is shown in Table 1. Röttger (in preparation) has described the given parameters in more detail. We note that the ESR and SSR have fairly equal system figures of merit. This results from the facts that the ESR has a more than one order of magnitude wider detection bandwidth to match the broader signal spectrum on 500 MHz (resulting in higher noise power), and from about ten times larger antenna aperture of the SSR (yielding higher signal levels). These counter-balance the higher system temperature and lower average power of the SSR as compared to the ESR. Since the signal-to-noise ratio of PMSE observed with the SSR can be to about 50 dB, we assumed that chances would exist to detect PMSE also with the ESR. This was proved by the first detection of PMSE with the ESR in July 1999.

In Fig. 5 height-time intensity plots (upper plots in the upper (ESR) and lower (SSR) panels) of a typical PMSE event are presented. The lower six/seven plots of the two panels show the dynamic spectra of the signals in the height ranges limited by the tick-marks on the left-hand side of the height-time-intensity plots. After about 1001 UT an enhancement was detected by the ESR with fairly wide spectra around 87–88 km and a much narrower spectra lower down at 86–87 km. The corresponding dynamic spectra of the SSR are shown in the lower panel of Fig. 5. We note some similarity in the occurrence of echoes of the SSR and the ESR. Closer inspection of temporal and spatial variations of the echoes (the SSR scans through five directions, which cover the one direction of the ESR beam) that these echoes, detected by the ESR and the SSR, result from the same irregularity structure, which was drifting horizontally through the observation area.

In Fig. 6 the spectra of the ESR signals are shown, which demonstrates the occurrence of broad and narrow spectrum widths. This means that there are two different irregularity structures, one is strongly turbulent (termed case 1 in Table 2, corresponding to the broad spectra in Fig. 6) and the other quite stable (which we annotate as non-turbulent; case 2 in

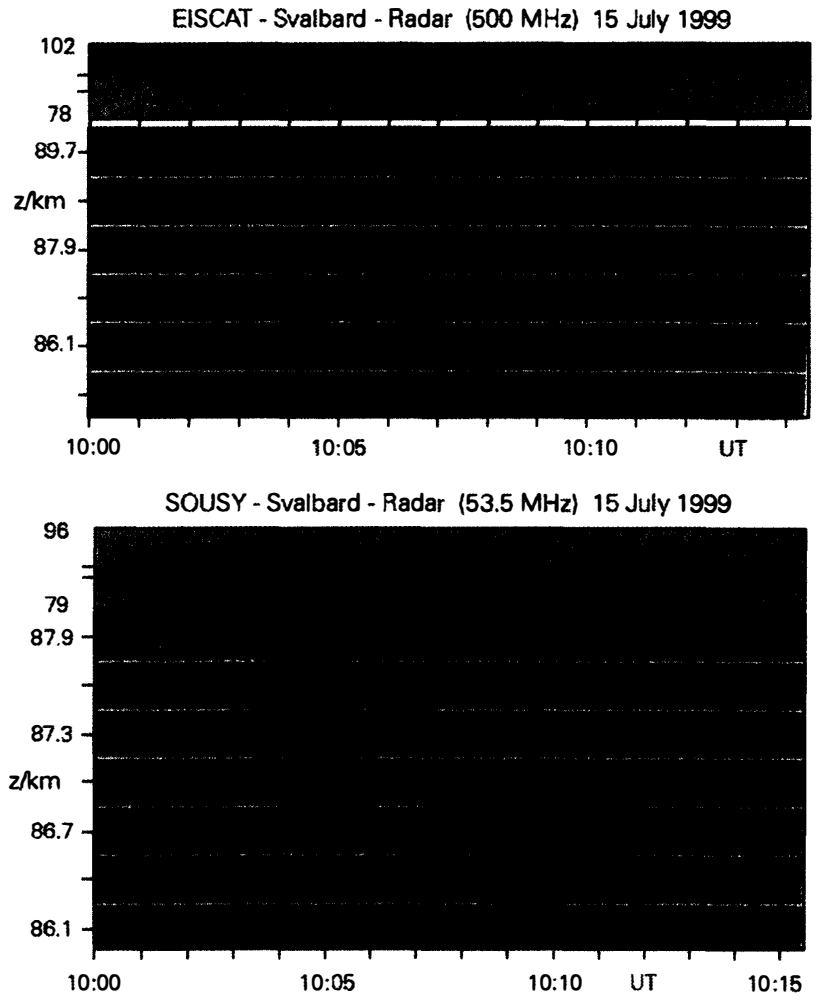

Fig. 5. Height-time-intensity plots and dynamic spectra of Polar Mesosphere Summer Echoes recorded with the EISCAT Svalbard Radar (upper panel) and the SOUSY Svalbard Radar (lower panel); from Röttger (2000).

Table 2, corresponding to the narrow spectra in Fig. 6), respectively. The ESR signal-to-noise ratio of the wide spectrum event is about 20%, and that of the narrow spectrum event is about 2%. Using proper system and noise calibration (Röttger, in preparation) we can estimate the received absolute signal power and convert that into radar reflectivity. This has been done for the given two events detected simultaneously by the ESR and the SSR. From the spectrum widths of the ESR we can also estimate the turbulence dissipation rate ε for an assumed reasonable Brunt-Väisälä frequency at these altitudes. The spectrum width is a measure for the turbulence energy dissipation rate, provided that antenna beam width and shear broadening is negligible. Since the beam width of the ESR of 1.23° is much narrower than that of the SSR (4°), we use the ESR spectrum widths to obtain the turbulence estimate. The electron density estimate N_e can be obtained from the background incoherent scatter signal as detected by the ESR (*e.g.,* Fig. 4). All these parameters are determining the radar reflectivity. Using the measured parameters (Table 2) and the system parameters

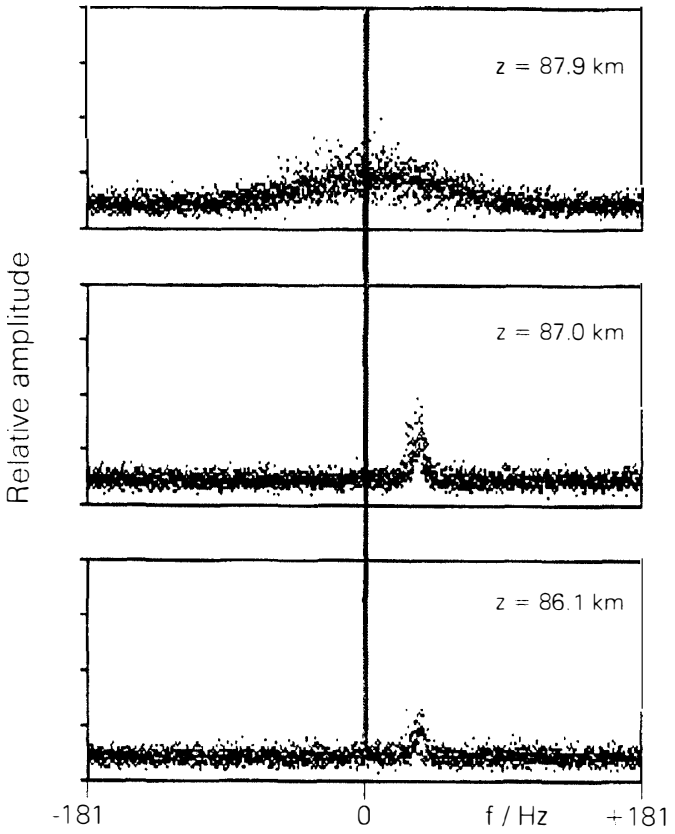

Fig. 6. Scatter plots of spectra of PMSE observed with the ESR, averaged over 90 s. Each single data point results from one 512-point spectrum taken over 1.4 s.

Table 2. Parameters deduced from radar observations during PMSE conditions.

	ESR	SSR		ESR	SSR
Case 1 (broad spectra, 87.9 km)			Case 2 (narrow spectra, 87.0 km)		
Received power in W	$1.6 \cdot 10^{-16}$	$1.2 \cdot 10^{-12}$		$1.0 \cdot 10^{-17}$	$1.0 \cdot 10^{-13}$
Radar reflectivity in m^{-1}	$5.3 \cdot 10^{-19}$	$2.2 \cdot 10^{-14}$		$3.3 \cdot 10^{-20}$	$1.8 \cdot 10^{-15}$
Turbulence energy dissipation rate ϵ in W kg^{-1}	0.26	(0.56)		0.01	(0.05)
Background electron density in m^{-3}	$5 \cdot 10^{8}$	–		$5 \cdot 10^{8}$	–

PMSE at 87–88 km height. Longyearbyen, 15 July 1999, 1002–1006 UT.

(Table 1), we can apply the technique of Hocking (1995) to deduce the radar volume reflectivity, which is the scatter cross section per unit volume, for the two cases of wide (case 1) and narrow (case 2) spectra.

6. Conclusion on ice particles in the polar summer mesopause

The spectral density of neutral turbulence need not to be identical with the spectrum of a passive scalar, such as free electrons in the *D*-region, mixed by this turbulence. The resulting deviations are determined by the Schmidt number $S_c = \nu/D$, where ν is the molecular viscosity of the neutral gas and D the diffusion coefficient of the electrons. The diffusion of the electrons is ambipolar and is controlled by the ions. Since massive ions are existent in the cold summer mesopause, it is expected that S_c can get much larger than one, which was suggested by Kelley *et al.* (1987) to be the cause for PMSE. Cho (1993) had

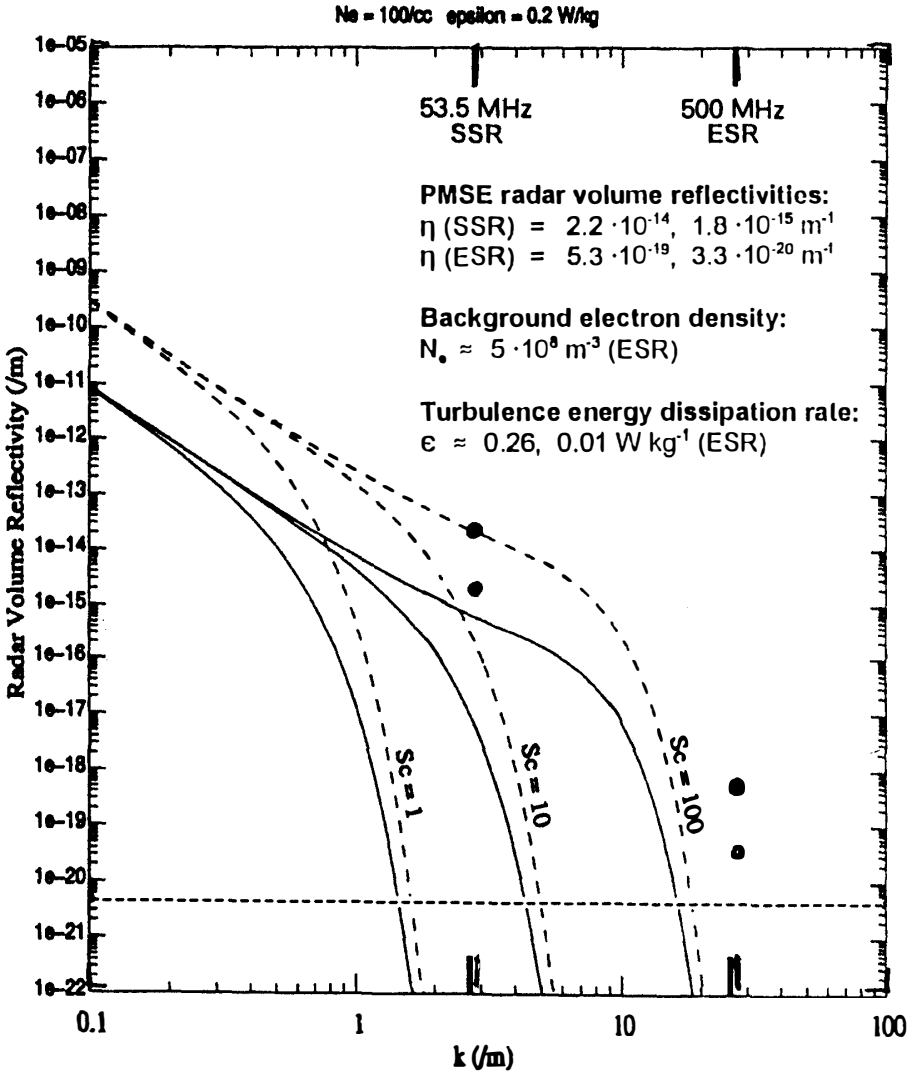

Fig. 7. Radar volume reflectivity of PMSE as function of wavenumber k for different Schmidt numbers S_c, calculated by Cho (1993). Included are the observed radar volume reflectivities η (for case 1 and case 2, see Table 2), and estimates of electron density N_e and turbulence energy dissipation rate ε deduced from the radar observations.

derived the radar volume reflectivity for different Schmidt numbers including the other controlling parameters, such as turbulence energy dissipation rate and the electron density. An example of Cho's diagrams is given in Fig. 7, which shows the radar volume reflectivity as function of wavenumber k. We have indicated here the Bragg wavenumbers of the SSR and the ESR. The radar volume reflectivities of the ESR and the SSR for the turbulent and non-turbulent echoes are shown by the full circles in Fig. 7. We note that the values deduced by our observations fit quite well into the calculations of Cho (1993) for the smaller wavenumber of the SSR. However, we need Schmidt numbers in excess of 100 to explain the relatively high volume reflectivities observed by the ESR.

The effective diffusion coefficient depends on the size and the charge number density of heavy ions or charged aerosol particles (*e.g.,* Hill, 1978). Cho (1993) had calculated the reduction of electron diffusion as function of aerosol or ice particles to electron density. We conclude from those calculations that particle radii would be in the order of a few tens of nanometers for Schmidt numbers larger than 100. The radii of ice particles, which are observed as Noctilucent Clouds and are considered essential for the creation of PMSE, are a few tens of nanometers (Klostermeyer, 1999). The results of our radar observations are compatible with these size distributions of ice particles in the high latitude summer mesopause. The intermittency of the PMSE layers observed in height and time (see Figs. 4 and 5) lets us assume that the ice particles, which are a prime reason for these echoes, occur in inhomogeneous layered structures, which are temporally intermittent and drift over the radars.

We have shown that the combination of two collocated and calibrated radars, operating at different frequencies, can provide significant proof that the electron diffusion in the polar summer mesopause is substantially reduced. This gives rise to enhancements of backscatter cross sections of PMSE. We also conjecture that the results of our two-radar observations are consistent with the presence of ice particle layers in the polar summer mesopause.

Acknowledgments

The author is indebted to his colleagues of the SOUSY project group collaborating in the SOUSY Svalbard Radar project. The EISCAT Svalbard Radar is funded by CNRS (France), MPG (Germany), NFR (Norway), NFR (Sweden), NIPR (Japan), PPARC (UK) and SA (Finland).

References

Balsley, B.B., Woodman, R.F., Sarango, M., Rodrigues, R., Urbina, J., Ragaini, E., Carey, J., Huaman, M. and Giraldez, A. (1995): On the lack of southern hemisphere polar mesosphere summer echoes. J. Geophys. Res., **100**, 11685–11693.

Bremer, J., Hoffmann, P., Manson, A.H., Meek, C.E., Rüster, R. and Singer, W. (1996): PMSE observations at three different frequencies in northern Europe during summer 1994. Ann. Geophys., **14**, 1317-1327.

Cho, J.Y.N. (1993): Radar scattering from the summer polar mesosphere: Theory and observations. Ph. D. dissertation, Cornell University, Ithaca, NY, USA, 181 p.

Cho, J.Y.N. and Röttger, J. (1997): An updated review of polar mesosphere summer echoes: Observations, theory, and their relations to noctilucent clouds and subvisible aerosols. J. Geophys. Res.,

102, 2001-2020.

Czechowsky, P., Klostermeyer, J., Röttger, J., Rüster, R. and Schmidt, G. (1988): The SOUSY Svalbard Radar for middle and lower atmosphere research in the polar region. Proc. 8th Workshop Techn. Sci. Aspects MST Radar, SCOSTEP, 318-321.

Hall, C.M. and Röttger, J. (2001): Initial observations of Polar Mesospheric Summer Echoes using the EISCAT Svalbard Radar. Geophys. Res. Lett., **28**, 131-134.

Hill, R.J. (1978): Nonneutral and quasi-neutral diffusion of weakly ionized miulti-constituent plasma. J. Geophys. Res., **83**, 989-998.

Hocking, W.K. (1995): Measurement of turbulent energy dissipation rates in the midle atmosphere by radar techniques: a review. Radio Sci., **20**, 1403-1422.

Kelley, M.C., Farley, D.T. and Röttger, J. (1987): The effect of cluster ions on anomalous VHF backscatter from the summer polar mesosphere. Geophys. Res. Lett., **14**, 1031-1034.

Klostermeyer, J. (1999): Physics of Polar Mesosphere Summer Echoes. Proc. 14th ESA Symposium on European Rocket and Balloon Programmes and Related Research, ESA SP-437, ESTEC, The Netherlands, 293-298.

Röttger, J. (1994a): Middle atmosphere and lower thermosphere processes at high latitudes studied with the EISCAT radars. J. Atmos. Terr. Phys., **56**, 1173-1195.

Röttger, J. (1994b): Polar Mesosphere Summer Echoes: Dynamics and Aeronomie of the Middle Atmosphere. Adv. Space Res., **14**(9), 123-138.

Röttger, J. (1997): Radar observations of the middle and lower atmosphere. Incoherent Scatter Theory, Practice and Science, ed. by D. Alcayde. EISCAT, 263-314 (Techn. Rep. **97/53**).

Röttger, J. (2000): Radar investigations of the mesosphere, stratosphere and the troposphere in Svalbard. Adv. Polar Upper Atmos. Res., **14**, 202-220.

Röttger, J. (2001): Observations of the Arctic troposphere and lower stratosphere with the SOUSY Svalbard Radar. Mem. Natl Inst. Polar Res., Spec. Issue, **54**, 1-8.

Röttger, J. and Tsuda, T. (1995): Studies of the polar middle and lower atmosphere by an MST radar on Svalbard. J. Geomagn. Geoelectr., **47**, 929-942.

Röttger, J., Rietveld, M.T., LaHoz, C., Hall, T., Kelley, M.C. and Swartz, W.E. (1990): Polar mesosphere summer echoes observed with the EISCAT 933-MHz radar and the CUPRI 46.9-MHz radar, their similarity to 224-MHz radar echoes and their relation to turbulence and electron density profiles. Radio Sci., **25**, 671-687.

Röttger, J., Markannen, J. and Wannberg, U.G. (1998): The EISCAT Svalbard Radar—Its potential for middle atmosphere studies. Proc. 8th Workshop Techn. Sci. Aspects MST Radar, SCOSTEP, 314-317.

Rüster, R., Röttger, J., Schmidt, G., Czechowsky, P. and Klostermeyer, J. (2001): Observations of Mesospheric Summer Echoes at VHF in the polar cap region. Geophys. Res. Lett., **28**, 1471-1474.

Wannberg, U.G., Wolf, I., Vanhainen, L.G., Koskeniemi, K., Röttger, J., Postila, M., Markannen, J., Jacobsen, R., Stenberg, A., Larsen, R., Eliassen, S., Heck, S. and Huuskonen, A. (1997): The EISCAT Svalbard Radar: A case study in modern incoherent scatter radar design. Radio Sci., **32**, 2283-2307.

(Received June 12, 2000; Revised manuscript accepted October 2, 2000)